A synchrotron powder X-ray diffraction study of the skutterudite-related phases AB1.5Te1.5 (A=Co, Rh, Ir; B= Ge, Sn)

Article

Accepted Version

A synchrotron powder X-ray diffraction study of the skutterudite-related phases $AB_{1.5}Te_{1.5}$ (A=Co, Rh, Ir; B= Ge, Sn)

Paz Vaqueiro,* Gerard G. Sobany and A.V. Powell

Department of Chemistry, Heriot-Watt University, Edinburgh EH14 4AS, UK

*Author for correspondence:
Dr P. Vaqueiro
Department of Chemistry
Heriot-Watt University
Edinburgh EH14 4AS
UK
Fax: +44 (0)131 451 3180
E-mail: chepv@hw.ac.uk

Graphical abstract:

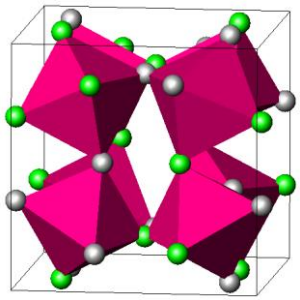

The ternary $AB_{1.5}Te_{1.5}$ phases adopt a skutterudite-related structure, containing diamond-shape B_2Te_2 rings, in which the B and Te atoms are ordered *trans* to each other.

Abstract

X-ray resonant scattering has been exploited to investigate the crystal structure of the $AB_{1.5}Te_{1.5}$ phases (A = Co, Rh, Ir; B = Ge, Sn). Analysis of the diffraction data reveals that $CoGe_{1.5}Te_{1.5}$ and $ASn_{1.5}Te_{1.5}$ adopt a rhombohedral skutterudite-related structure, containing diamond-shape B_2Te_2 rings, in which the B and Te atoms are ordered and *trans* to each other. Anion ordering is however incomplete, and with increasing the size of both cations and anions, the degree of anion ordering decreases. By contrast, the diffraction data of $IrGe_{1.5}Te_{1.5}$ are consistent with an almost statistical distribution of the anions over the available sites, although some ordered domains may be present. The thermoelectric properties of these materials are discussed in the light of these results.

Introduction

The skutterudite structure (space group $Im\bar{3}$), which is adopted by binary compounds with the general formula MX_3 (M = Co, Rh or Ir and X = P, As or Sb), can be described as a distorted ReO_3 structure, in which the cations retain their octahedral coordination while the anions form four-membered rings (Figures 1(a) and 1(b)).[1] There are two large cages per unit cell, which can be filled to varying degrees by up to one atom per formula unit according to $G_xM_4X_{12}$, where the guest ion G can be a rare-earth, actinide, alkaline-earth, alkali metal or thallium cation.[2] By replacing M or X with electron-deficient elements, complete filling of the cages (x=1) can be achieved. Very recently, a family of superconducting filled skutterudites GPt_4Ge_{12} (G = rare-earth or alkaline-earth metal), in which the pnictogen has been replaced by germanium, has been reported.[3]

Many binary skutterudites exhibit high mobilities and Seebeck coefficients, whilst low thermal conductivities are found upon insertion of filler atoms. As a consequence, skutterudites offer great potential for thermoelectric applications at elevated temperatures, and in recent years, the thermoelectric properties of filled antimony-based skutterudites have been extensively investigated.[2] The range of available skutterudite compositions can be however expanded quite considerably by preparing ternary unfilled phases. Ternary unfilled skutterudites can be obtained by substitution at the anion or the cation site. Isoelectronic substitution at the cation site, by a pair of elements from groups 8 and 10, results in the formation of phases such as $Fe_{0.5}Ni_{0.5}Sb_3$[4] and $Ru_{0.5}Pd_{0.5}Sb_3$,[5] whilst isoelectronic substitution at the anion site results in the family of materials with general formula $AB_{1.5}Q_{1.5}$ (A = Co, Rh, Ir; B = Ge, Sn; Q = S, Se, Te).[6] Simultaneous substitution at both the anion and the cation sites is also possible, as exemplified by the compound $FeSb_2Te$.[6(c)] Much of our recent work has centered on the structural characterisation and the thermoelectric properties

of the family of ternary skutterudites $AB_{1.5}Q_{1.5}$. In contrast with the ternary skutterudites formed by cation substitution, which are isostructural to the binary phases,[4,5] our structural studies, carried out using high-resolution powder neutron diffraction, reveal that $CoGe_{1.5}Te_{1.5}$[7] and $AGe_{1.5}S_{1.5}$ (A = Co, Rh, Ir)[8] adopt an ordered variant of the skutterudite structure (space group $R\bar{3}$), in which the anions are ordered in layers perpendicular to the [111] direction of the skutterudite unit cell (Figures 1(c) and 1(d)). Recent reports of the existence of the phases $G_xCo_4Ge_4Q_4$ (G = Ce, Yb; Q = Se, Te),[9,10] indicate that these ternary skutterudites may also be filled. Since the unit cells of many of the $AB_{1.5}Q_{1.5}$ phases are metrically cubic, and their structures contain neighbouring elements (e.g. Ge/Se, Sn/Te), investigation of anion ordering using conventional powder X-ray diffraction is difficult, and reported structures are based on heavily constrained refinements.[11] In an effort to elucidate the detailed crystal structure of the tellurium-containing skutterudites $AB_{1.5}Te_{1.5}$, we have carried out a high-resolution synchrotron powder X-ray diffraction experiment. In order to increase the contrast between the anions, we have exploited X-ray resonant scattering, using data collected at different wavelengths, near to and far from the Sn and Te edges. The transport properties of the $AB_{1.5}Te_{1.5}$ phases were previously reported by us.[12]

Experimental

Synthesis

The compounds $CoGe_{1.5}Te_{1.5}$, $CoSn_{1.5}Te_{1.5}$, $RhSn_{1.5}Te_{1.5}$, $IrGe_{1.5}Te_{1.5}$ and $IrSn_{1.5}Te_{1.5}$ were prepared from appropriate stoichiometric mixtures of the elements cobalt (Aldrich, 99.9%), rhodium (Goodfellow, 99.9%), iridium (Aldrich, 99.9%), germanium (Aldrich, 99.99%), tin (Johnson Matthey, 99.9%) and tellurium (Aldrich

99.997%). Prior to use, Ge powder was reduced in a stream of H_2/Ar at 500ºC to remove GeO_2. Each ternary mixture was ground in an agate mortar prior to sealing into an evacuated (<10^{-4} Torr) silica tube. The inner wall of the silica tube was coated with a thin layer of carbon by pyrolysis of acetone. Each reaction mixture was heated at 430ºC for 2 days, followed by 2 additional days at 580ºC. Samples were cooled to room temperature at 0.1ºC min^{-1}, prior to removal from the furnace. Following re-grinding, samples were sealed into a second carbon-coated silica tube and refired at 580°C for 2 days, followed by cooling to room temperature at 0.1ºC min^{-1}. The progress of the reactions was monitored by powder X-ray diffraction, using a Philips PA2000 diffractometer with nickel-filtered Cu-Kα radiation (λ = 1.5418 Å). For the tin-containing samples, one or two additional firings at 580ºC were required to ensure complete reaction.

Diffraction data collection and analysis

High-resolution powder X-ray diffraction data were collected at the European Synchrotron Radiation Facility, beam line ID31, at room temperature. The samples were loaded into borosilicate glass capillaries, mounted on the diffractometer and spun at 50 Hz during measurements in order to improve powder randomisation. Two datasets, far from an adsorption edge (0.42704(1) Å) and close to it, were collected for each sample. Wavelengths of 0.38970(6) Å and 0.4249(1) Å, close to the tellurium and tin K-edges were used for the germanium and tin-containing samples respectively. X-ray fluorescence spectra were collected near the K-edges of tin and tellurium, and used as input for the program Chooch,[13] in order to determine the resonant scattering factors. For each sample, two datasets were simultaneously used in Rietveld refinements, which were performed using the GSAS package.[14]

Results

Conventional powder X-ray diffraction data collected on bulk samples of composition $CoGe_{1.5}Te_{1.5}$, $IrGe_{1.5}Te_{1.5}$ and $ASn_{1.5}Te_{1.5}$ (A = Co, Rh, Ir) are consistent with the formation of skutterudite-type phases. Data could be indexed on the basis of a pseudo-cubic unit cell with $a \approx 8.7$-9.3 Å. However, attempts to prepare "$RhGe_{1.5}Te_{1.5}$" resulted always in samples containing a mixture of GeTe and $RhTe_2$ and a ternary phase subsequently identified by us as RhGeTe.[15] Examination of the synchrotron diffraction data for the $AB_{1.5}Te_{1.5}$ phases under investigation, indicated that all prepared materials contain trace amounts of binary tellurides, as well as binary oxides in some cases, while the $RhSn_{1.5}Te_{1.5}$ sample contains a significant amount of $RhTe_2$ (*ca.* 14 wt%). The binary phases contained in each sample are listed in Table 1.

For several skutterudite-related phases of the type $AB_{1.5}Q_{1.5}$, it has been observed[6(a)] that the powder diffraction patterns contain weak reflections which violate the body-centring condition $h+k+l = 2n$ of the ideal skutterudite structure (see ESI[§]). These additional reflections can be indexed on the basis of the previously reported ordered skutterudite structure.[7,8] Examination of the synchrotron powder diffraction data reveals that these reflections are clearly present in $CoGe_{1.5}Te_{1.5}$ as well as in the three $ASn_{1.5}Te_{1.5}$ phases, and therefore the atomic coordinates of the ordered skutterudite structure[7,8] were used for the initial structural model in the Rietveld refinements. Whilst in the ideal cubic skutterudite structure the B and Te atoms are statistically distributed over the 24(*g*) site, in the ordered skutterudite structure there are four crystallographically distinct anion sites. The use of resonant X-ray scattering enabled us to investigate the distribution of the B and Te atoms over these four anion sites. In addition to the refinement of background terms, peak shape parameters, phase fractions, lattice parameters, thermal parameters and atomic parameters, anion site occupancy factors were introduced as variables into the refinements, with the

constraint that the overall stoichiometry was maintained. The final refined parameters are presented in Table 1, while observed, calculated and difference profiles for the diffraction data are shown in Figure 2. Selected distances and angles are given in Table 2.

In the powder diffraction pattern of $IrGe_{1.5}Te_{1.5}$ there are a small number of weak and broad features which violate the body-centering condition of the ideal skutterudite structure but could be indexed using the ordered skutterudite unit cell. The full width at half maximum of these broad features is *ca.* 0.2-0.3º, considerably larger than that of the intense reflections (*ca.* 0.02º). This anisotropic broadening of powder X-ray diffraction peaks could be ascribed to anionic disorder. For this reason, Rietveld refinements using the ideal skutterudite (space group $Im\bar{3}$) and the ordered skutterudite (space group $R\bar{3}$) models were attempted. The refinement in $R\bar{3}$ did not result in a significantly better agreement between observed and calculated data, despite the larger number of refined parameters, and the inclusion of anisotropic broadening parameters for the peak shape description. The refined parameters for $IrGe_{1.5}Te_{1.5}$ in the ideal skutterudite structure are presented in Table 3, while selected distances and angles are given in Table 4. Final observed, calculated and difference profiles are shown in Figure 3.

Given the difficulties involved in discriminating between neighbouring elements using conventional powder X-ray diffraction, the distribution of B and Q atoms over the four available anion sites in the ordered skutterudite structure has only been investigated previously for the $AGe_{1.5}S_{1.5}$ phases, using powder neutron diffraction (as Ge and S have markedly different neutron scattering cross sections of 8.42 and 1.02 barns, respectively). Almost complete ordering of the anions was found, with only a small percentage (*ca.* 5% or less, depending on the nature of A) of Ge atoms residing

at the S atom sites.[8] By contrast, for the tellurium-containing phases reported here, the percentage of B atoms residing on Te sites varies over the range 12-30% depending upon chemical composition. A clear trend can be observed in the anion distribution (Table 1); with increasing size of both cations and anions, the degree of disorder increases. For instance, whilst in $CoGe_{1.5}Te_{1.5}$ only 12% of Ge atoms reside on Te sites, in $IrGe_{1.5}Te_{1.5}$ there is an almost statistical distribution of Ge and Te atoms, although some short-range ordering may occur. In the fully ordered skutterudite structure, there is a strict alternation of B and Te layers, perpendicular to the [111] direction. Given the recently reported skutterudites containing Ge_4 rings,[3] we may speculate that the anion disorder found in the $AB_{1.5}Q_{1.5}$ phases might be related to stacking faults in the sequence of B and Te layers. This may explain the anisotropic broadening of peaks observed in $IrGe_{1.5}Te_{1.5}$.

In the fully ordered skutterudite structure, each transition metal is octahedrally coordinated by three B and three tellurium atoms, arranged in a facial configuration. A similar octahedral arrangement, with each type of anion defining a face of the octahedron, has been found in the ternary AGeTe phases (A = Co, Rh).[15] Instead of the rectangular anion rings characteristic of binary skutterudites,[16] the structure of the ordered skutterudites investigated here contains two crystallographically-independent diamond-shape B_2Te_2 rings, in which the B and Te atoms are *trans* to each other (Figure 4). The Te-B-Te angles within the rings for the ordered skutterudites described here are in the range 82.12-87.15(13)º (Table 2), whilst the B-Te-B angles are always greater than 90º. As the size of the anion or the cation increases, these angles tend towards the ideal value (90º) found in MX_3-type skutterudites.

Discussion

Skutterudites are sometimes described as Zintl phases,[17] and use of the Zintl formalism for the $AB_{1.5}Te_{1.5}$ phases investigated here results in formal charges of B^{2-} and Te^0 for the anions. This would result in a formulation $A^{3+}{}_4[B_2Te_2]^{4-}{}_3$, in which the transition-metal cation has a d^6 configuration. A d^{10} configuration of the transition metal would also be consistent with the diamagnetic behaviour of ternary skutterudites.[6(a)] Classical Zintl phases consist of electropositive cations and complex anionic units, which can be isolated clusters or extended units. However, in the $AB_{1.5}Te_{1.5}$ phases, the electronegativities of all elements are comparable, and Ge and Sn are the least electronegative elements when A is Rh or Ir (Pauling electronegativities: Ge, 2.01; Sn, 1.96; Co, 1.88; Rh, 2.28; Ir, 2.2; Te, 2.1).[18] This suggests that an electron counting scheme based on the Zintl formalism is not valid, a view which is supported by electronic structure calculations on $CoSn_{1.5}Te_{1.5}$ which indicate that cobalt is negatively charged.[19]

The electrical and thermal transport properties of the $AB_{1.5}Te_{1.5}$ phases are summarised in Table 5. It has been previously reported that the thermal conductivity of a number of ternary skutterudites is greatly reduced when compared with that of the binary phases.[6(c), 20] Our own thermal conductivity measurements yield values (at 325 K) of 3.0, 2.3 and 1.3 $Wm^{-1}K^{-1}$ for $CoGe_{1.5}S_{1.5}$, $CoGe_{1.5}Te_{1.5}$ and $CoSn_{1.5}Te_{1.5}$ respectively.[21] These are significantly lower than that of $CoSb_3$ (10.5 $Wm^{-1}K^{-1}$).[2] Anion ordering will have a major effect on the phonon dispersion curves and the corresponding phonon density of states (DOS), as a consequence of the lower crystal symmetry of the ordered skutterudite when compared with the ideal skutterudite structure ($R\bar{3}$ vs. $Im\bar{3}$). Comparison of the reported infrared spectra of $CoAs_3$ with those of the ternary skutterudites $AGe_{1.5}Q_{1.5}$[22] provides evidence of a marked increase in the number of lattice vibrations. Calculations of phonon dispersion curves, which

are being currently carried out by M. Fornari and co-workers, are expected to shed some light on this aspect.[23] Our analysis of the synchrotron diffraction data for $AB_{1.5}Te_{1.5}$ phases indicates that, in addition to a lowering of crystal symmetry, there is a degree of disorder in the anion rings. This will result in an increase in point-defect scattering, and therefore in reduced thermal conductivities. A similar reduction in thermal conductivity upon introduction of disorder in the pnictogen rings has been observed in the filled skutterudite $LaIr_4Ge_3Sb_9$.[24] Other types of structural disorder, such as the combination of vacancies and interstitial Zn atoms found in β-Zn_4Sb_3,[25] also result in reduced thermal conductivities.

The reduction in thermal conductivity found in the $AB_{1.5}Te_{1.5}$ phases is accompanied by a significant increase in their electrical resistivity[12] from that of the binary phases. Indeed, it has been generally found that substitution in the pnictogen rings of skutterudites has a deleterious effect on the electronic properties.[2] In the case of the materials reported here, such large electrical resistivities may be associated with the increased ionicity of the bonding,[23] particularly within the B_2Q_2 rings. Extended Hückel tight-binding calculations[26,27] on MX_3 phases indicate that the top of the valence band is formed by π-type X_4 orbitals, which are strongly mixed with the *d* orbitals of the transition metal.[28] Bonding within homonuclear X_4 rings is purely covalent. However, owing to the different electronegativities of B and Q, in the heteronuclear B_2Q_2 rings, changes in the electron distribution within the available π-type orbitals of the rings occur,[28] together with changes in the band dispersion at the top of the valence band.[23]

Tight-binding calculations for $CoGe_{1.5}Q_{1.5}$ (Q = S, Se) suggest that *dπ-pπ* bonding between Ge and Co atoms is responsible for the diamond-shape distortion of the Ge_2Q_2 rings.[29] For the ternary phases described here, *dπ-pπ* bonding may account for

the distortion of the B_2Q_2 rings, as well as for the larger A-B-A angles when compared to A-Q-A angles. However, such π bonding is likely to be weaker for materials containing elements from later periods, and therefore both the distortion of the B_2Q_2 rings and the degree of anion ordering may be related to the *d*π-*p*π bonding strength. This is consistent with the observed trends: with increasing size of both cations and anions the B_2Q_2 geometry tends towards the rectangular geometry of the ideal skutterudite structure, and the degree of anion disorder increases. Structural trends as well as the electronic behaviour of a number of intermetallic compounds have also been found to be dependent on the strength of *d*π-*p*π bonding.[30]

Conclusions

Although the $AB_{1.5}Te_{1.5}$ phases adopt an ordered skutterudite structure, analysis of X-ray resonant diffraction data reveals that anion ordering is not complete. This structural disorder is likely to be a contributory factor in the low thermal conductivities found for these phases, whilst their larger electrical resistivities may arise as a result of the increased ionicity within the B_2Q_2 rings when compared to the homonuclear pnictogen rings of binary skutterudites.

Acknowledgements

We acknowledge the European Synchrotron Radiation Facility for provision of synchrotron radiation facilities and we would like to thank Dr Irene Margiolaki for assistance in using beamline ID31. PV thanks the UK EPSRC for an Advanced Research Fellowship (GR/S54982/01).

[§] Electronic Supplementary Information (ESI) available: Diffraction profiles over the region 6-15º.

References

1. R. H. Mitchell, Perovskites: Modern and Ancient, (Almaz Press, 2002)

2. C. Uher, in M.G. Kanatzidis, S. D. Mahanti and T. P. Hogan (Ed.), Chemistry, Physics and Materials Science of Thermoelectric Materials: beyond Bismuth Telluride, Kluwer Academics/Plenum Publishers, New York, 2003, p. 121.

3. (a) E. Bauer, A. Grytsiv, X. Q. Chen, N. Melnychenko-Koblyuk, G. Hilscher, H. Kaldarar, H. Michor, E. Royanian, G. Giester, M. Rotter, R. Podloucky, P. Rogl, *Phys. Rev. Lett.*, 2007, **99**, 217001; (b) R. Gumeniuk, W. Schnelle, H. Rosner, M. Nicklas, A. Leithe-Jasper, Y. Grin, *Phys. Rev. Lett.*, 2008, **100**, 017002.

4. A. Kjekshus, D. G. Nicholson, T. Rakke, *Acta Chem. Scand.*, 1973, **27**, 1315-1320.

5. T. Caillat, J. Kulleck, A. Borshchevsky, J.-P. Fleurial, *J. Appl. Phys.*, 1996, **79**, 8419-8426.

6. (a) R. Korenstein, S. Soled, A. Wold, G. Collin, *Inorg. Chem.*, 1977, **16**, 2344-2346; (b) A. Lyons, R. P. Gruska, C. Case, S. N. Subbarao, A. Wold, *Mat. Res. Bul.*, 1978, **13**, 125-128; (c) J.-P. Fleurial, T. Caillat and A. Borshchevsky, *Proceedings of the 16th International Conference on Thermoelectrics*, Dresden, Germany, 1997, p. 1-11.

7. P. Vaqueiro, G. G. Sobany, A. V. Powell and K. S. Knight, *J. Solid State Chem.*, 2006, **179**, 2047-2053.

8. P. Vaqueiro, G. G. Sobany and M. Stindl, *J. Solid State Chem.*, 2008, **181**, 768-776.

9. Q. Lin, A. L. E. Smalley, D. C. Johnson, J. Martin, G. S. Nolas, *Chem. Mater.*, 2007, **19**, 6615-6620.

10. J. Navrátil, T. Plecháček, L. Beneš, M. Vlček, F. Laufek, *Proc. 5th Europ. Conf. Thermoelectrics*, Odessa, Ukraine, 2007, 52.

11. J. W. G. Bos, R. J. Cava, *Solid State Commun*., 2007, **141**, 38-41.

12. P. Vaqueiro and G. G. Sobany, in Thermoelectric Power Generation, edited by T.P. Hogan, J. Yang, R. Funahashi, and T. Tritt (Mater. Res. Soc. Symp. Proc. Volume 1044, Warrendale, PA, 2008), 185-190.

13. G. Evans and R. F. Pettifer, *J. Appl. Crystallogr.*, 2001, **34**, 82-86.

14. A. C. Larson, R. B. von Dreele, *General Structure Analysis System*, Los Alamos Laboratory, [Report LAUR 85-748], 1994.

15. P. Vaqueiro, G. G. Sobany, F. Guinet and P. Leyva-Bailen, *Solid State Sci.*, 2009**,** **11**, 1077-1082.

16. (a) A. Kjekshus, D. G. Nicholson, T. Rakke, *Acta Chem. Scand.*, 1973, **27**, 1307-1314; (b) A. Kjekshus, T. Rakke, *Acta Chem. Scand.*, 1974, **28**, 99-103.

17. S. M. Kauzlarich, S. R. Brown, G. J. Snyder, *Dalton Trans.*, 2007, 2099-2107.

18. L. Pauling, *The Nature of the Chemical Bond*, 3rd edition, Cornell University Press, Itaca, NY, 1960.

19. L. Bertini, S. Cenedese, *Phys. Stat. Sol.(RRL)*, 2007, **1**, 244-246.

20. (a) G. S. Nolas, J.Yang, R. W. Ertenberg, *Phys. Rev. B*, 2003, **68**, 193206; (b) Y. Nagamoto, K. Tanaka, T. Koyanagi, *Proceedings of the 16th International Conference on Thermoelectrics*, Dresden, Germany, 1997, 330-333.

21. These values, which have been taken from ref.12, have been corrected from the effect of the porosity of the samples, using the procedure described in ref. 15.

22. H. D. Lutz and G. Kliche, *J. Solid State Chem.*,1981, **40**, 64-68.

23. D. Volja, M. Fornari, B. Kozinsky, N. Marzari, in Materials and Devices for Thermal-to-Electric Energy Conversion, edited by J. Yang, G.S. Nolas, K. Koumoto, Y. Grin (Mater. Res. Soc. Symp. Proc. Volume 1166, Warrendale, PA, 2009), 1166-N05-04.

24. G. S. Nolas, G. A. Slack, D. T. Morelli, T. M. Tritt, A. C. Ehrlich, *J. Appl. Phys.*, 1996, **79**, 4002.

25. F. Cargnoni, E. Nishibori, P. Rabiller, L. Bertini, G. J. Snyder, M. Christensen, C. Gatti, B. B. Iversen, *Chem.-Eur. J.*, 2004, **10**, 3862-3870.

26. D. Jung, M.-H. Whangbo, S. Alvarez, *Inorg. Chem.*, 1990, **29,** 2252-2255.

27. M. Llunell, P. Alemany, S. Alvarez, V.P. Zhukov, A. Vernes, *Phys. Rev. B*, 1996, **53**,10605-10609.

28. M. Partik, H. D. Lutz, *Phys. Chem. Minerals*, 1999, **27**, 41-46.

29. M. Partik, C. Kringe, H. D. Lutz, *Z. Kristallogr.*, 1996, **211,** 304-312.

30. (a) D. A. Pankhurst, D. Nguyen-Manh, D. G. Pettifor, *Phys. Rev. B*, 2004, **69**, 075113; (b) U. Häussermann, M. Elding-Pontén, C. Svensson, S. Lidin, *Chem. Eur. J.*, 1998, **4**, 1007-1015.

Figure Captions

Figure 1	Comparison of the ideal skutterudite (MX_3) and the ordered skutterudite ($AB_{1.5}Q_{1.5}$) structures (a) Polyhedral representation of MX_3 structure. (b) Ball and stick representation of MX_3 structure, showing the planar rectangular four-membered X_4 rings. (c) Polyhedral representation of $AB_{1.5}Q_{1.5}$ structure. (d) Ball and stick representation of $AB_{1.5}Q_{1.5}$ structure. Key: M, open circles; X, black circles; A, open circles; B, black circles; Q, grey circles.
Figure 2	Final observed (crosses), calculated (full line) and difference (lower full line) diffraction profiles for (a) $CoGe_{1.5}Te_{1.5}$ (upper plot: λ = 0.42704(1) Å, lower plot: λ = 0.38970(6) Å) (b) $CoSn_{1.5}Te_{1.5}$ (upper plot: λ = 0.42704(1) Å, lower plot: λ = 0.4249(1) Å) (c) $RhSn_{1.5}Te_{1.5}$ (upper plot: λ = 0.42704(1) Å, lower plot: λ = 0.4249(1) Å), and (d) $IrSn_{1.5}Te_{1.5}$ (upper plot: λ = 0.42704(1) Å, lower plot: λ = 0.4249(1) Å). Reflection positions are marked: the lower markers refer to the skutterudite phase and the upper markers to the impurity phases listed in Table 1.
Figure 3	Observed (crosses), calculated (upper full line) and difference (lower full line) profiles for $IrGe_{1.5}Te_{1.5}$, collected on the ID31 beamline at room temperature: (a) λ = 0.42704(1) Å and (b) λ = 0.38970(6) Å. The insets show reflections at shorter d-spacings. Reflection positions are marked: the lower markers refer to $IrGe_{1.5}Te_{1.5}$, middle markers to Ir and the upper markers to GeO_2.
Figure 4	The four-membered rings in $CoSn_{1.5}Te_{1.5}$. Key: Sn, black circles; Te, grey circles.

Table 1

Final refined parameters for materials with the ordered skutterudite structure (space group $R\bar{3}$). All atoms on 18(*f*): (*x,y,z*), except for A(1) on 6(*c*): (*0,0,z*). The weight percentages of other phases included in the refinements are shown.

		$CoGe_{1.5}Te_{1.5}$	$CoSn_{1.5}Te_{1.5}$	$RhSn_{1.5}Te_{1.5}$	$IrSn_{1.5}Te_{1.5}$
a/Å		12.33239(3)	12.90916(2)	13.16485(6)	13.19386(4)
c/ Å		15.10650(7)	15.78585(4)	16.1241(1)	16.1672(1)
A(1)	*z*	0.2462(8)	0.2522(3)	0.2499(5)	0.2506(3)
	B/Å^2	0.258(9)	0.225(9)	0.330(7)	0.283(3)
A(2)	*x*	0.6681(8)	0.6680(4)	0.6665(5)	0.6666(3)
	y	0.8329(5)	0.8358(2)	0.8338(3)	0.8335(1)
	z	0.5812(3)	0.5871(1)	0.5854(2)	0.5845(1)
	B/Å^2	0.258(9)	0.225(9)	0.330(7)	0.283(3)
B(1)	SOF Ge/Sn	0.880(2)	0.850(4)	0.820(7)	0.695(11)
	SOF Te	0.120(2)	0.150(4)	0.180(7)	0.305(11)
	x	0.8359(3)	0.8371(1)	0.8356(5)	0.8361(5)
	y	0.9941(2)	0.9976(1)	0.0001(4)	0.0072(4)
	z	0.1603(2)	0.16051(8)	0.1623(4)	0.1630(3)
	B/Å^2	0.599(3)	0.589(3)	0.585(5)	0.681(6)
B(2)	SOF Ge/Sn	0.880(2)	0.850(4)	0.820(7)	0.695(11)
	SOF Te	0.120(2)	0.150(4)	0.180(7)	0.305(11)
	x	0.9451(2)	0.9475(1)	0.9432(5)	0.9441(3)
	y	0.2163(4)	0.2167(2)	0.2128(5)	0.2136(4)
	z	0.5557(1)	0.55291(6)	0.5573(3)	0.5559(2)
	B/Å^2	0.599(3)	0.589(3)	0.585(5)	0.681(6)
Q(1)	SOF Ge/Sn	0.120(2)	0.150(4)	0.180(7)	0.305(11)
	SOF Te	0.880(2)	0.850(4)	0.820(7)	0.695(11)
	x	0.9345(2)	0.9380(1)	0.9355(4)	0.9358(3)
	y	0.2136(3)	0.2166(1)	0.2167(4)	0.2146(4)
	z	0.0657(1)	0.06214(5)	0.0647(3)	0.0649(2)
	B/Å^2	0.599(3)	0.589(3)	0.585(5)	0.681(6)
Q(2)	SOF Ge/Sn	0.120(2)	0.150(4)	0.180(7)	0.305(11)
	SOF Te	0.880(2)	0.850(4)	0.820(7)	0.695(11)
	x	0.8382(2)	0.8373(1)	0.8357(4)	0.8356(4)
	y	0.0174(2)	0.01169(8)	0.0151(4)	0.0133(3)
	z	0.6657(2)	0.66618(7)	0.6658(3)	0.6654(3)
	B/Å^2	0.599(3)	0.589(3)	0.585(5)	0.681(6)
Weight Percentage/%		$CoTe_2$ 4.45(4)	SnTe 2.31(3) $Co_{0.63}Te$ 2.81(3)	$RhTe_2$ 14.33(5)	SnTe 2.47(5) Ir_3Te_8 5.15(4) Ir 0.6(1)
R_{wp}/%	Histogram 1[a]	6.79	7.03	7.73	8.37
	Histogram 2[b]	5.77	5.74	6.72	6.96

[a] Data collected at λ = 0.42704(1) Å.

[b] Data collected at λ = 0.38970(6) Å for $CoGe_{1.5}Te_{1.5}$ and at λ = 0.4249(1) Å for the remaining samples.

Table 2

Selected bond distances (Å) and angles (º) for the ordered skutterudites $AB_{1.5}Te_{1.5}$.

	$CoGe_{1.5}Te_{1.5}$	$CoSn_{1.5}Te_{1.5}$	$RhSn_{1.5}Te_{1.5}$	$IrSn_{1.5}Te_{1.5}$
A(1)-B(1)	2.375(7) × 3	2.541(3) × 3	2.585(7) × 3	2.627(5) × 3
A(1)-Q(2)	2.496(7) × 3	2.532(2) × 3	2.645(7) × 3	2.638(5) × 3
B(1)-A(1)-B(1)	93.0(4) × 3	90.76(12) × 3	93.00(27) × 3	93.63(17) × 3
B(1)-A(1)-Q(2)	90.75(8) × 3 82.32(9) × 3	88.95(4) × 3 83.82(3) × 3	88.25(16) × 3 82.84(17) × 3	86.32(13) × 3 84.16(13) × 3
Q(2)-A(1)-Q(2)	94.23(34) × 3	96.41(11) × 3	95.96(24) × 3	95.88(17) × 3
A(2)-B(1)	2.336(6)	2.532(4)	2.568(6)	2.615(5)
A(2)-B(2)	2.379(5) 2.391(6)	2.523(4) 2.541(3)	2.597(6) 2.620(7)	2.591(5) 2.599(4)
A(2)-Q(1)	2.525(6) 2.518(5)	2.537(2) 2.559(3)	2.628(6) 2.642(6)	2.651(4) 2.650(5)
A(2)-Q(2)	2.537(5)	2.555(4)	2.651(6)	2.650(5)
B(1)-A(2)-B(2)	89.67(11) 87.73(12)	86.33(6) 86.47(7)	85.79(18) 87.47(17)	85.83(12) 87.25(14)
B(1)-A(2)-Q(1)	96.47(29) 89.59(23)	95.27(13) 90.79(15)	97.10(19) 92.26(19)	96.02(15) 93.39(17)
B(2)-A(2)-B(2)	94.20(28)	90.68(13)	91.30(21)	91.54(14)
B(2)-A(2)-Q(1)	88.28(12) 83.31(13)	88.84(8) 83.63(7)	87.53(21) 83.94(19)	88.42(13) 84.01(12)
B(2)-A(2)-Q(2)	96.65(25) 92.11(26)	96.29(16) 91.84(12)	95.65(20) 92.32(20)	95.54(16) 92.11(14)
Q(1)-A(2)-Q(1)	94.26(25)	96.92(13)	97.21(21)	96.06(16)
Q(1)-A(2)-Q(2)	83.44(11) 84.11(9)	86.44(7) 86.43(6)	84.86(18) 84.48(15)	84.63(14) 85.20(12)
B(1)-Q(1)	2.748(4) 2.941(4)	2.9019(14) 3.0865(20)	2.931(5) 3.049(7)	2.852(6) 3.007(5)
Q(1)-B(1)-Q(1)	82.12(10)	84.95(4)	84.74(19)	87.15(13)
B(1)-Q(1)-B(1)	97.88(10)	95.05(4)	95.26(19)	92.85(13)
B(2)-Q(2)	2.698(4) 2.864(4)	2.9087(15) 3.0789(20)	2.856(5) 3.052(7)	2.896(6) 3.094(5)
Q(2)-B(2)-Q(2)	84.50(10)	85.16(4)	85.75(21)	85.73(12)
B(2)-Q(2)-B(2)	95.50(10)	94.84(4)	94.25(21)	94.27(12)

Table 3

Final refined parameters for $IrGe_{1.5}Te_{1.5}$ (space group $Im\bar{3}$, a = 8.95621(4) Å, R_{wp} = 9.63 and 6.97% for data collected at λ = 0.42704(1) Å and λ = 0.38970(6) Å respectively). The site occupancy factors of Ge and Te, located on the 24(*g*) site, were fixed at 50%. Ir (0.87(2)wt%) and GeO_2 (0.25(2)wt%) were included in the refinement.

Atom	Site	*x*	*y*	*z*	B/Å^2
Ir	8(*c*)	1/4	1/4	1/4	0.469(6)
Ge/Te	24(*g*)	0	0.85098(9)	0.65844(9)	1.01(1)

Table 4
Selected bond distances (Å) and angles (º) for $IrGe_{1.5}Te_{1.5}$.

Ir-Ge/Te	2.5502(3) × 6
B-Ir-B	94.88(3) × 6 85.13(3) × 6
B-B	2.838(2) 2.669(2)

Table 5

Electrical resistivity (ρ), Seebeck coefficient (S) and thermal conductivity (κ), at room temperature, for the $AB_{1.5}Te_{1.5}$ phases.[12]

Formula	ρ/Ωcm	S/μVK^{-1}	κ/Wm^{-1}K^{-1}
$CoGe_{1.5}Te_{1.5}$	5.1	-713	2.3[a]
$IrGe_{1.5}Te_{1.5}$	7.6	243	-
$CoSn_{1.5}Te_{1.5}$	5.9	-309	1.3[a]
$RhSn_{1.5}Te_{1.5}$[b]	0.01	53	-
$IrSn_{1.5}Te_{1.5}$	0.3	125	-

[a] Value measured at 325 K. [b] Sample contains *ca.* 14% $RhTe_2$.

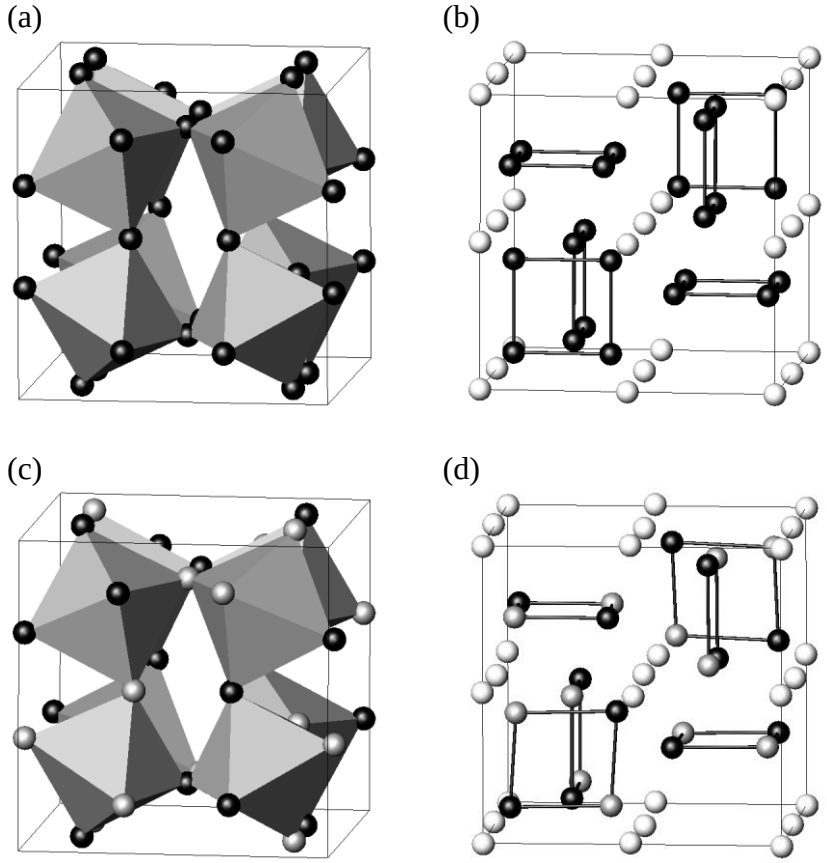

Figure 1

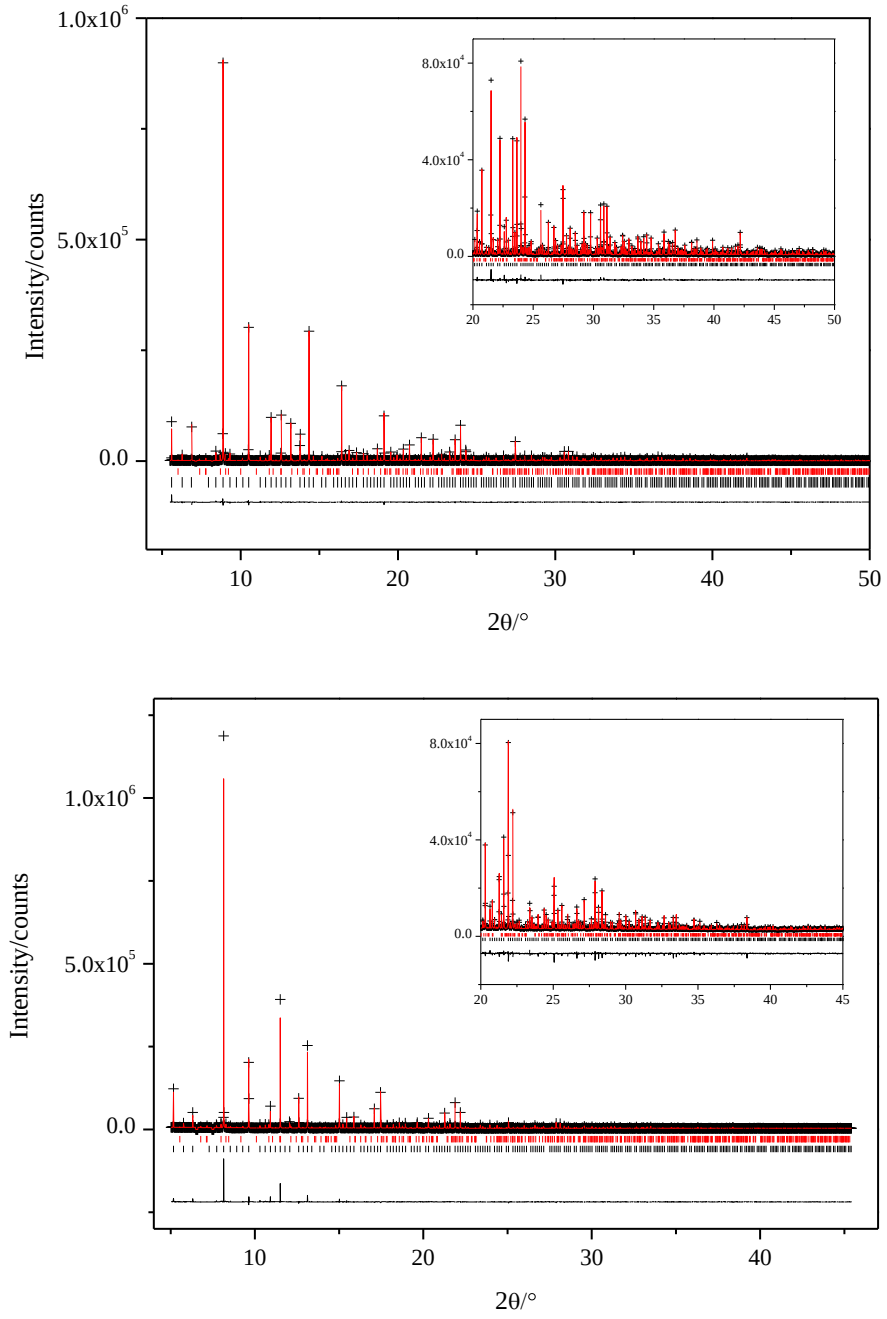
1.0x10^6
5.0x10^5
0.0
Intensity/counts
10
20
30
40
50
2θ/°
8.0x10^4
4.0x10^4
0.0
20
25
30
35
40
45
50

1.0x10^6
5.0x10^5
0.0
Intensity/counts
10
20
30
40
2θ/°
8.0x10^4
4.0x10^4
0.0
20
25
30
35
40
45

Figure 2(a)

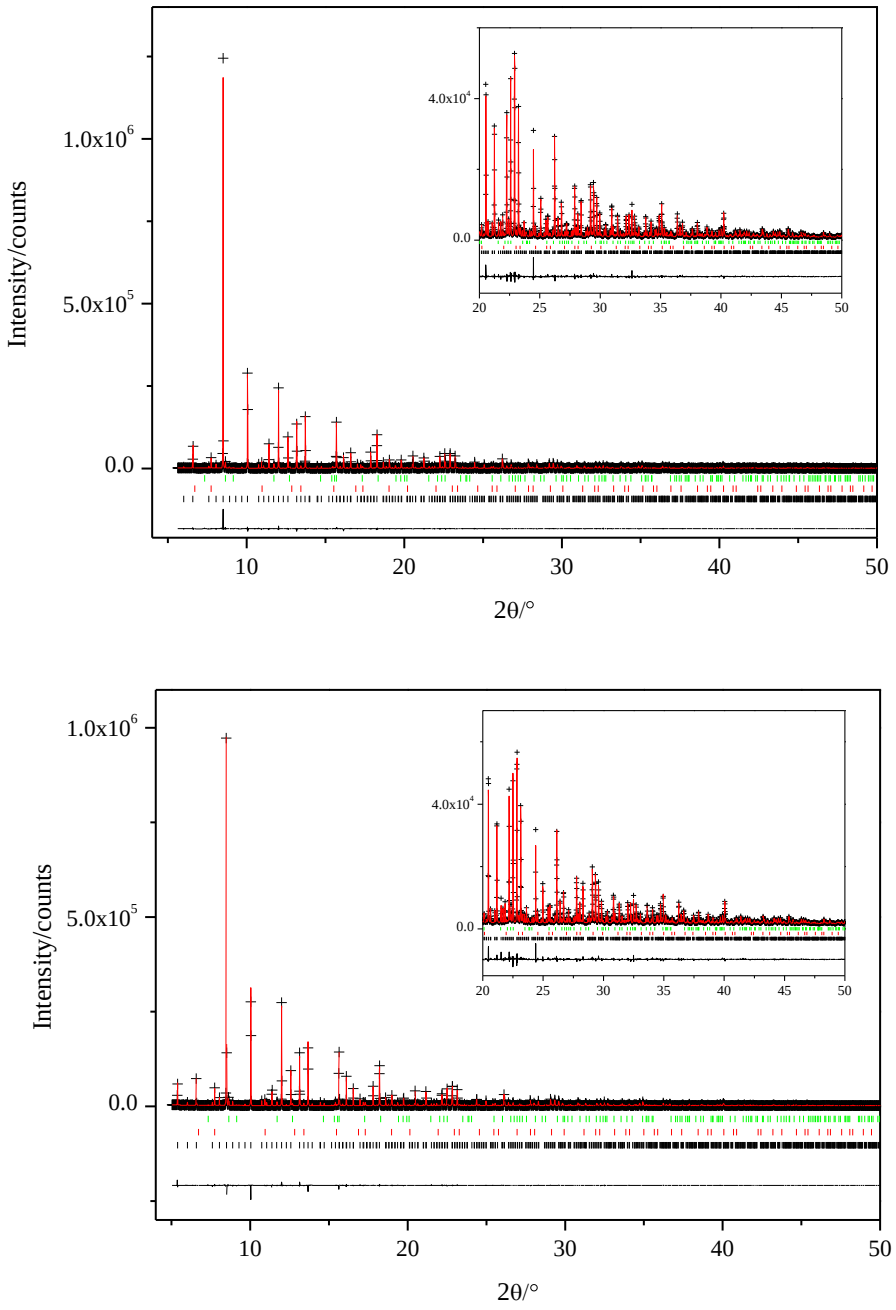
Intensity/counts
1.0x10^6
5.0x10^5
0.0
4.0x10^4
0.0
10
20
30
40
50
2θ/°
Intensity/counts
1.0x10^6
5.0x10^5
0.0
4.0x10^4
0.0
10
20
30
40
50
2θ/°

Figure 2(b)

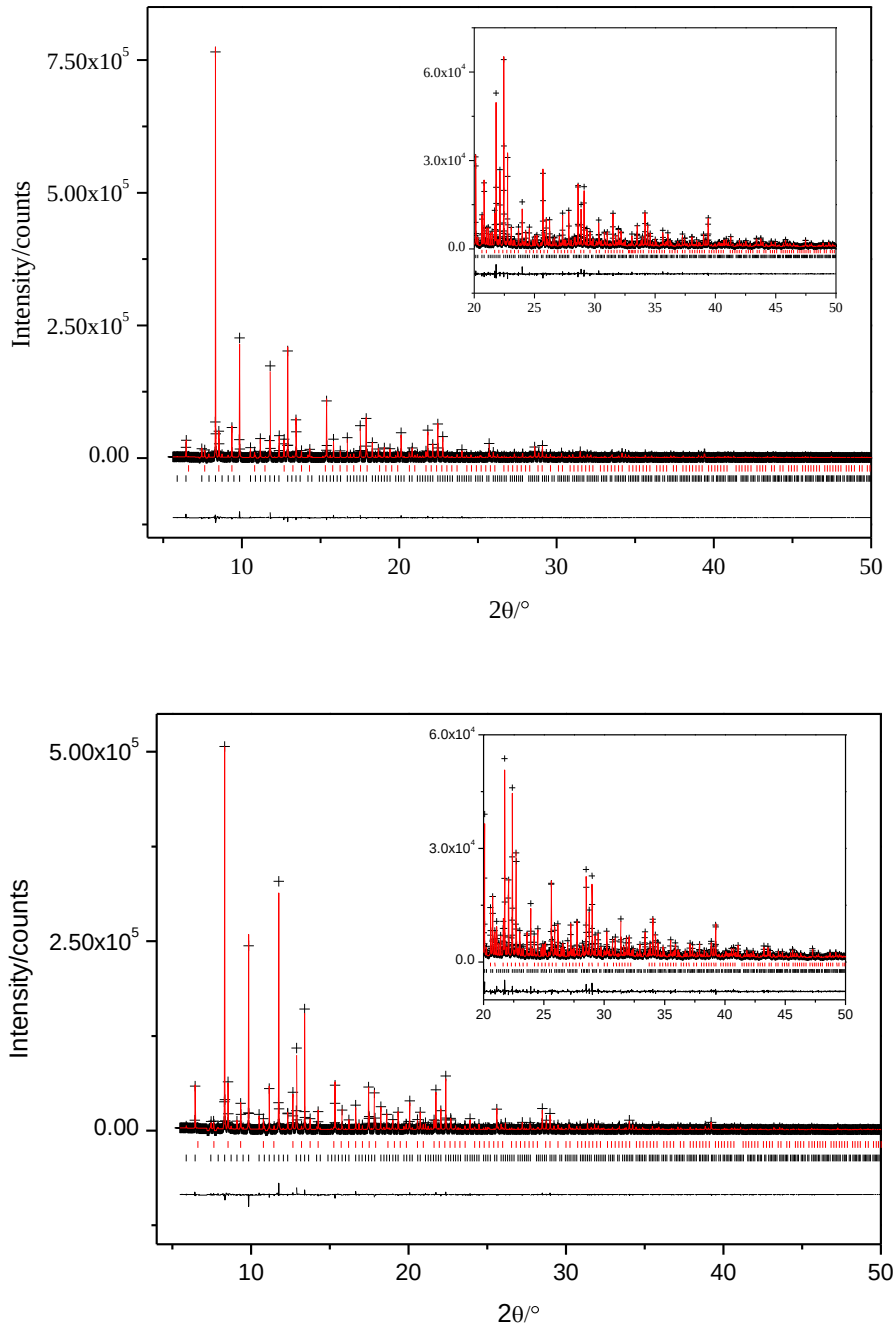
Intensity/counts
7.50x10^5
5.00x10^5
2.50x10^5
0.00
10
20
30
40
50
2θ/°
6.0x10^4
3.0x10^4
0.0
20
25
30
35
40
45
50
Intensity/counts
5.00x10^5
2.50x10^5
0.00
10
20
30
40
50
2θ/°
6.0x10^4
3.0x10^4
0.0
20
25
30
35
40
45
50

Figure 2(c)

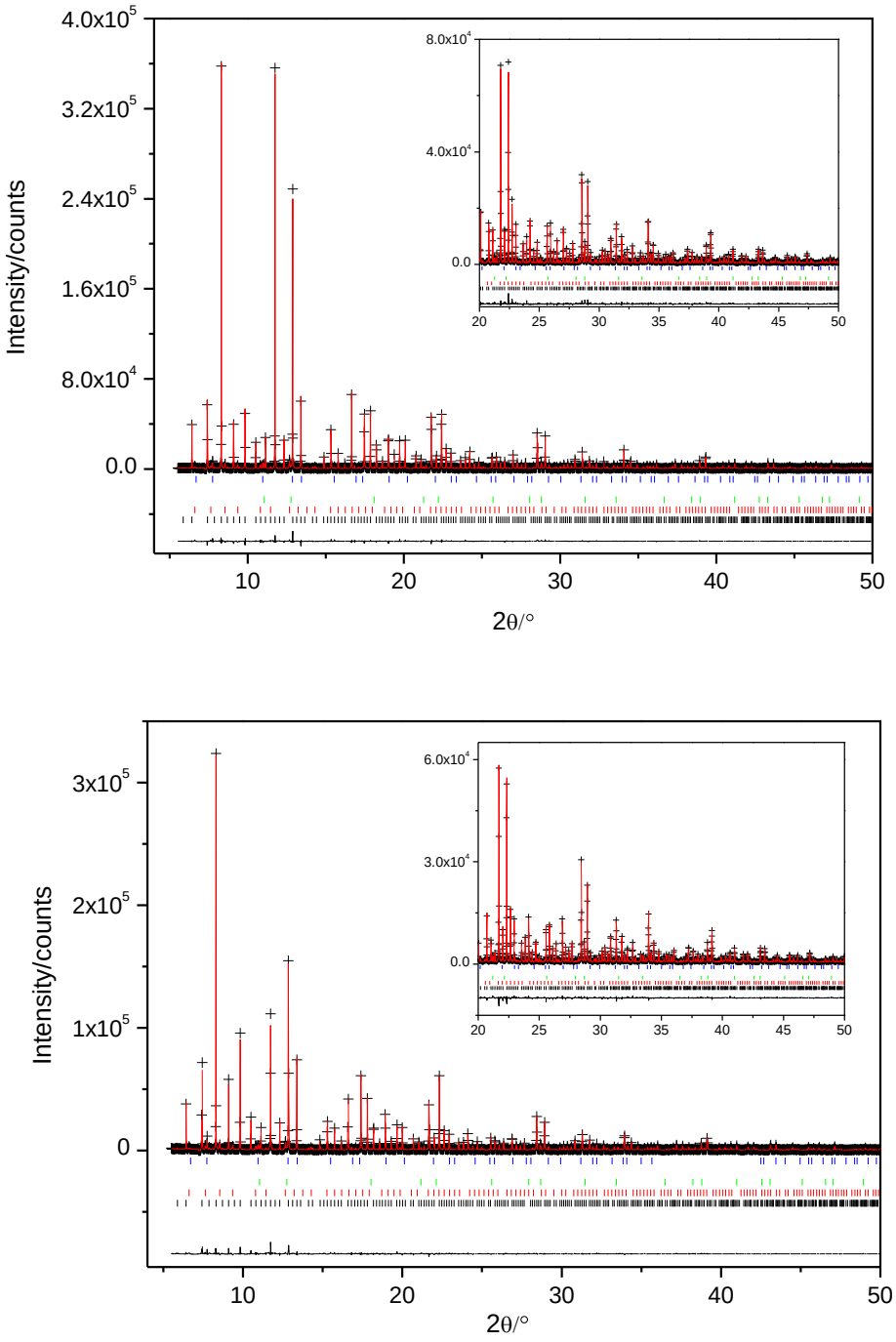
Intensity/counts
2θ/°
4.0x10^5
3.2x10^5
2.4x10^5
1.6x10^5
8.0x10^4
0.0
10
20
30
40
50
8.0x10^4
4.0x10^4
0.0
20
25
30
35
40
45
50
Intensity/counts
2θ/°
3x10^5
2x10^5
1x10^5
0
6.0x10^4
3.0x10^4
0.0

Figure 2(d)

(a)

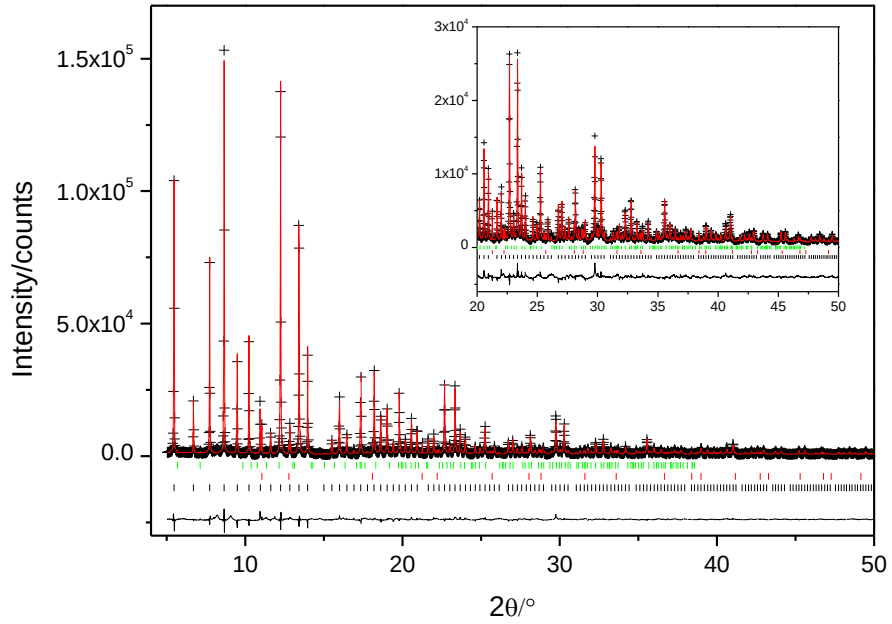
Intensity/counts
1.5x10^5
1.0x10^5
5.0x10^4
0.0
10
20
30
40
50
2θ/°
3x10^4
2x10^4
1x10^4
0
20
25
30
35
40
45
50

(b)

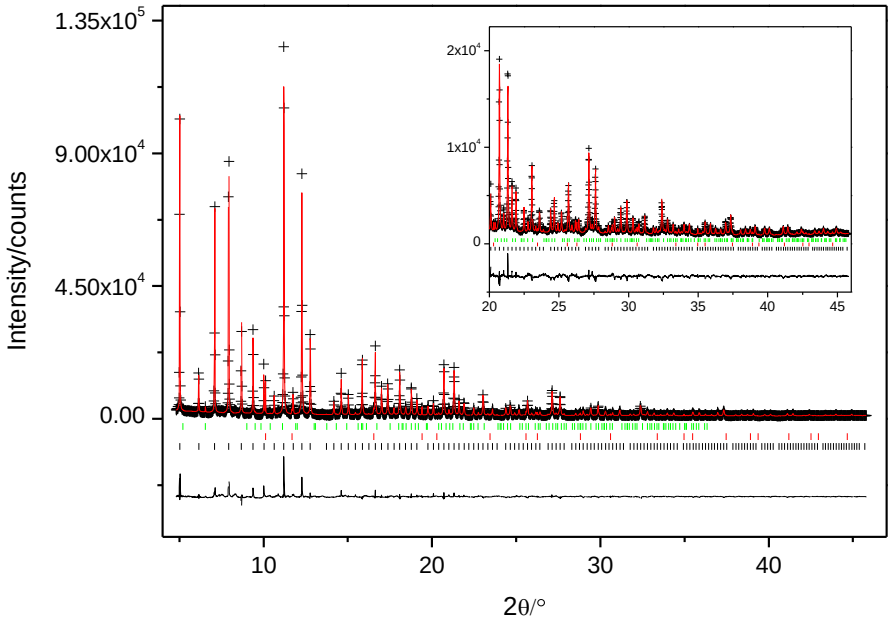
Intensity/counts
1.35x10^5
9.00x10^4
4.50x10^4
0.00
10
20
30
40
2θ/°
2x10^4
1x10^4
0
20
25
30
35
40
45

Figure 3

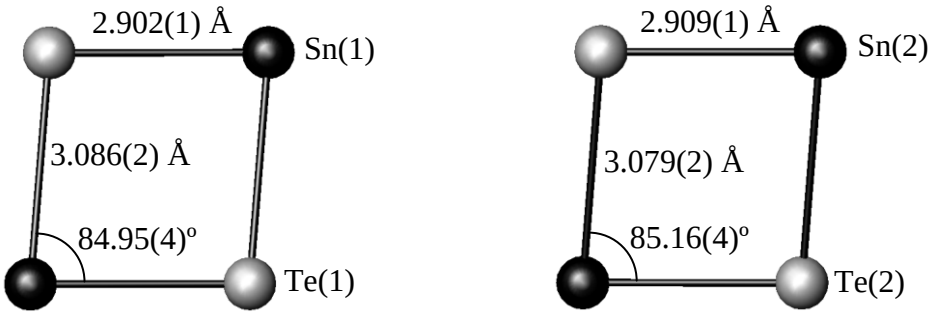

Figure 4